Short Communication

Crystal structure of the mouse hepatitis virus ns2 phosphodiesterase domain that antagonizes RNase L activation

Baokun Sui,[1]† Junhua Huang,[1]† Babal K. Jha,[2] Ping Yin,[3] Ming Zhou,[1] Zhen F. Fu,[4] Robert H. Silverman,[2] Susan R. Weiss,[5] Guiqing Peng[1] and Ling Zhao[1]

Correspondence
Guiqing Peng
penggq@mail.hzau.edu.cn
Ling Zhao
lingzhao@mail.hzau.edu.cn

[1]State Key Laboratory of Agricultural Microbiology, College of Veterinary Medicine, Huazhong Agricultural University, Wuhan 430070, PR China

[2]Department of Cancer Biology, Lerner Research Institute, Cleveland Clinic, Cleveland, OH 44195, USA

[3]National Key Laboratory of Crop Improvement, Huazhong Agricultural University, Wuhan 430070, PR China

[4]Department of Pathology, University of Georgia, Athens, GA 30602, USA

[5]Department of Microbiology, Perelman School of Medicine, University of Pennsylvania, Philadelphia, PA 19104, USA

Received 6 October 2015
Accepted 8 January 2016

Prior studies have demonstrated that the mouse hepatitis virus (MHV) A59 strain ns2 protein is a member of the 2H phosphoesterase family and exhibits 2′,5′-phosphodiesterase (PDE) activity. During the IFN antiviral response, ns2 cleaves 2′,5′-oligoadenylate (2-5A), a key mediator of RNase L activation, thereby subverting the activation of RNase L and evading host innate immunity. However, the mechanism of 2-5A cleavage by ns2 remains unclear. Here, we present the crystal structure of the MHV ns2 PDE domain and demonstrate a PDE fold similar to that of the cellular protein, a kinase anchoring protein 7 central domain (AKAP7^{CD}) and rotavirus VP3 carboxy-terminal domain. The structure displays a pair of strictly conserved HxT/Sx motifs and forms a deep, positively charged catalytic groove with β-sheets and an arginine-containing loop. These findings provide insight into the structural basis for 2-5A binding of MHV ns2.

Innate immunity, which is commonly triggered by dsRNA in eukaryotic cells, plays a crucial role in viral defence (Wang & Carmichael, 2004). The 2′,5′-oligoadenylate (2-5A) synthase (OAS)/RNase L system, which is one of the most effective IFN-induced antiviral pathways, utilizes several strategies to inhibit viral infections (Silverman, 2007). Viruses induce the production of type I IFN, resulting in the activation of hundreds of IFN-stimulated genes, including four or more OAS genes (Der *et al.*, 1998; Kristiansen *et al.*, 2011; Schindler & Darnell, 1995; Stark *et al.*, 1998). OASs 1–3 use ATP to synthesize a series of 2-5A molecules consisting of [$p_3A(2'p5'A)n$, $n \geq 2$] upon stimulation by viral dsRNA (Hovanessian & Justesen, 2007; Kerr & Brown, 1978). These 2-5A molecules bind to the N-terminal ankyrin repeat and central protein kinase-like domains of RNase L, causing inactive RNase L monomers to form activated dimers with potent RNase activity that preferentially cleave single-stranded viral or cellular RNA after UU and UA repeats (Cole *et al.*, 1997; Dong & Silverman, 1995; Han *et al.*, 2014; Huang *et al.*, 2014).

Both coronavirus and rotavirus families include pathogens that can lead to severe diseases in humans and animals (Desselberger, 2014; Zaki *et al.*, 2012). Prior studies have reported that coronavirus mouse hepatitis virus (MHV) and group A rotavirus (RVA) encode ns2 and VP3 proteins, respectively. Ns2 and VP3 carboxy-terminal domain (CTD) belong to the 2H phosphoesterase superfamily, containing two conserved HxT/Sx motifs (where H represents histidine and x denotes a hydrophobic residue). Both ns2 and VP3 display 2′,5′-phosphodiesterase (PDE) activity, which can inhibit the activation of RNase L through degradation of its activator 2-5A, thereby

†These authors contributed equally to this work.

Atomic coordinates and structure factor amplitudes for MHV-A59 ns2$^{7-167}$ have been deposited in the Protein Data Bank (PDB) under accession code 4Z5V.

One supplementary table is available with the online Supplementary Material.

antagonizing the OAS/RNase L pathway and evading host innate immunity (Zhang *et al.*, 2013; Zhao *et al.*, 2012). AKAP7 is a member of the AKAP family that localizes to nuclei and has a central domain (esidues 87-292, AKAP7^{CD}) that belongs to the 2H phosphoesterase superfamily. AKAP7 exhibits 2′,5′-PDE activity that can complement an inactive MHV ns2 gene and degrade 2-5A with kinetics similar to that of MHV ns2 (Gold *et al.*, 2008; Gusho *et al.*, 2014). Although from different origins, these proteins display 2′,5′-PDE activity and can prevent the activation of RNase L by cleaving 2-5A.

To further elucidate the mechanism by which MHV ns2 binds and cleaves 2-5A, we resolved the crystal structure of the PDE domain of MHV-A59 ns2. The full-length ns2 protein containing residues 1–261 readily aggregates, possibly due to its cysteine-rich (six cysteines in a 62 aa segment, approximately 10 %) carboxy-terminal region. Thus, to select an ns2 fragment suitable for crystallization, we designed a series of C-terminally truncated constructs of ns2 based on a secondary structure prediction for this protein. An ns2 fragment containing residues 1–199 (ns2$^{1–199}$) including the PDE activity domain (residues 6–186) exhibited improved expression and solubility compared with the full-length protein (Fig. 1a, b and data not shown). To purify the ns2$^{1–199}$ protein, the codon-optimized sequence of truncated MHV-A59 ns2$^{1–199}$ was cloned into pET-42b vector (Novagen) with a 6 × His tag at the C terminus. Expression of ns2$^{1–199}$ protein was induced in *Escherichia coli* Rosetta BL21(DE3) (at an OD_{600} of 0.7) with 0.5 mM IPTG. After incubation for 18 h at 18 °C, the cells were collected and homogenized in PBS. After centrifugation at 10 000 ***g*** for 10 min, the supernatant was applied to Ni^{2+} affinity resin (Ni-NTA; GE) and further purified by gel filtration chromatography on Superdex 75 (GE Healthcare). The final protein preparation (at 10 mg ml^{-1}) containing 20 mM Tris/HCl (pH 7.4) and 200 mM NaCl was crystallized using the hanging-drop vapour-diffusion method at 4 °C with a reservoir solution containing 16 % (w/v) polyethylene glycol 3350, 0.1 M succinic acid (pH 7.0) and 20 mM hexamminecobalt(III) chloride. Selenomethionine (SeMet)-labelled protein was overexpressed in M9 minimal salts, and purified in the same way as the unmodified protein. The first crystal appeared 2 days post-seeding and the crystals were harvested for X-ray diffraction analysis 2 weeks later. However, the resolution was not high enough for data collection (3.6 Å), so dehydration was applied according to the protocols described by Heras & Martin (2005). The crystals were soaked in dehydration buffer containing 0.5 M succinic acid (pH 7.0) and 25 % polyethylene glycol 3350 for 1 month. Diffraction data were collected at the Shanghai Synchrotron Radiation Facility (SSRF) and then integrated and scaled using the HKL2000 package (Otwinowski & Minor, 1997). The structure of ns2$^{1–199}$ was determined by single-wavelength anomalous diffraction (SAD) phasing using SeMet-labelled ns2$^{1–199}$ and four SeMet sites in ns2$^{1–199}$ were identified. Model building and refinement were iteratively conducted using PHENIX and COOT (Adams *et al.*, 2002; Emsley & Cowtan, 2004). Data collection and refinement statistics for the ns2$^{1–199}$ crystal structure are provided in Table S1 (available in the online Supplementary Material). The ns2$^{1–199}$ structure was determined to within 3.05 Å. Since the residues of 1–6 and 168–199 were disordered and could not be resolved, we chose the ordered region (residues 7–167) as the final model, defined as ns2$^{7–167}$ (Fig. 1c–e).

To our knowledge, the crystal structure of the PDE domain of ns2 is the first coronavirus 2′,5′-PDE structure to be reported. Based on an overview of the structure of ns2$^{7–167}$, we found that this protein features a globular α/β-type architecture consisting of three α-helices and nine β-sheets with approximate dimensions of 48 Å × 46 Å × 16 Å (Fig. 1c, d). The structure is bilobal, with β1/2/3/5/6/7/9 and an arginine (R)-containing loop (R-loop, the loop between α3 and β7) that forms a concave surface where the electrostatic potential is positive and presumed to be the domain in which the negatively charged 2-5A binds and is cleaved (Fig. 1e) (Gold *et al.*, 2008). In accordance with the definition of the 2H phosphoesterase family, the β3 strand harbours an HxSx (where x is a hydrophobic residue) motif, and the β7 strand harbours an HxTx motif (Fig. 2a, b). This pair of HxT/Sx motifs play a key role in 2′,5′-PDE activity and are conserved in the ns2 homologues of other group 2a betacoronaviruses, including human virus OC43 and toroviruses (Silverman & Weiss, 2014). Prior research has demonstrated that mutations at the catalytic residues H46 and H126 in conserved HxT/Sx motifs of ns2 abolish PDE activity *in vitro* and severely impact virus replication *in vivo* (Zhao *et al.*, 2011, 2012).

MHV ns2, VP3-CTD and AKAP7^{CD} are representative 2H phosphoesterases (Fig. 1a) (Gusho *et al.*, 2014; Zhang *et al.*, 2013; Zhao *et al.*, 2012). Based on the sequence alignment, we identified a number of conserved residues in these 2H phosphoesterases (Fig. 2a). The structures of AKAP7^{CD} (PDB ID 2VFY) and VP3-CTD (PDB ID 5AF2), which exhibit substantial structural homology, have previously been determined (Brandmann & Jinek, 2015; Ogden *et al.*, 2015). The structural alignment of ns2$^{7–167}$, AKAP7^{CD} and VP3-CTD indicated that all of these structures form similar positive electrostatic concave regions in the 2′,5′-PDE activity domain, which is putatively involved in the binding and cleavage of 2-5A (Fig. 2b, c). In addition, the two conserved HxT/Sx motifs at the H46/S48/H126/T128 residues of ns2 were located in positions similar to those of the H132/T134/H224/T226 residues of AKAP7^{CD} and the H718/T720/H797/T799 residues of VP3-CTD (Fig. 2d). The arginine that is important for stabilizing 2-5A has previously been reported to be present in the R-loop region and is also strictly conserved in those three proteins (Fig. 2a, d) (Ogden *et al.*, 2015). All of the aforementioned characteristics demonstrate the structural conservation of the PDE catalytic domain of these three 2H phosphoesterases, despite lacking significant sequence homology (Fig. 2a).

Both MHV ns2 and RVA VP3 are viral proteins that display 2′,5′-PDE activity, although there are subtle differences

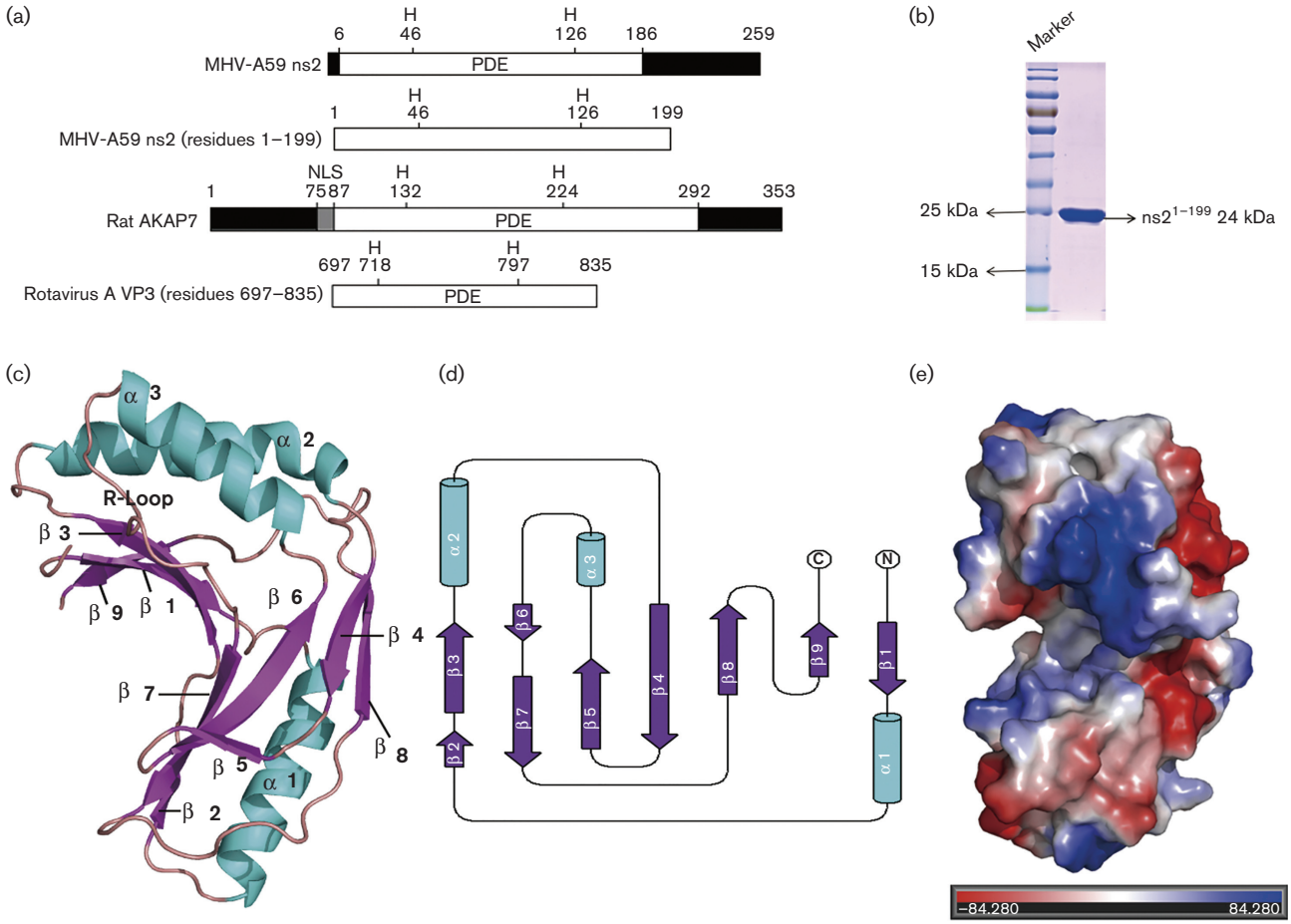

Fig. 1. An overview of the ns2$^{7–167}$ structure and the PDE domains of ns2, AKAP7 and VP3. (a) The 2′,5′-PDE activity domains of ns2, AKAP7 and VP3. NLS, Nuclear localization signal. (b) Purified ns2$^{1–199}$ protein used for crystallization. The molecular mass of purified ns2$^{1–199}$ protein was consistent with the expected size of 24 kDa and the purity was greater than 95 % (SDS-PAGE). (c) Overview of the structure of ns2$^{7–167}$. Colours and numbers indicate secondary structural elements of ns2$^{7–167}$. Structure figures were generated by PyMOL. (d) Schematic of the secondary structure components of ns2$^{7–167}$. The diagram was generated using CCP4-TopDraw with α-helices, β-strands and other secondary structure components coloured blue, green and black, respectively. Figures are not drawn to scale. (e) The protein molecule of ns2$^{7–167}$ coloured according to the electrostatic surface potential (calculated with APBS).

between the ns2$^{7–167}$ and VP3-CTD structures. The ns2$^{7–167}$ structure displays α-helices in the region from S19 to M35 (α1), which is similar to AKAP7^{CD}, whereas VP3-CTD shows a loop in this region that is much shorter compared with ns2$^{7–167}$ (Fig. 2b). The regions from residues D79 to D83 (β4) and Y144 to P148 (β8) display two β-sheets that are similar to those of AKAP7^{CD}, whereas the similar regions of VP3-CTD show two loops. Although some differences are seen between ns2$^{7–167}$ and VP3-CTD, these two proteins show greater structural similarities in their PDE catalytic domains between themselves than compared with AKAP7^{CD} [AKAP7^{CD}, with a root mean square deviation (RMSD) of 2.41 Å between the 149 Cα atoms. VP3-CTD, with the RMSD of 1.67 Å between the 148 Cα atoms. Analysed by PDBeFold.], having nearly identical β sheet coordinates (β1/3/6/7) (Fig. 2e). Prior studies have demonstrated that the L758 residue plays a key role in VP3-CTD activity (Ogden *et al.*, 2015); ns2$^{7–167}$ has an L88 in this position, although AKAP7^{CD} contains a Q residue in this position (Fig. 2a). Two α-helices at the position of α2/α3 in ns2$^{7–167}$ are also conserved in these three proteins, although ns2 and VP3 have shorter α-helices in α3 than does AKAP7^{CD}. The sequence alignment of ns2$^{1–199}$, VP3-CTD and AKAP7^{CD} illustrates that ns2$^{1–199}$ and VP3-CTD share greater sequence homology compared with AKAP7^{CD} (Fig. 2a). According to these features, we can conclude that ns2$^{7–167}$ not only displays structural features of AKAP7^{CD} but also of VP3-CTD, and ns2$^{7–167}$ shares greater sequence or structural homology with VP3-CTD compared with AKAP7^{CD}.

It has previously been reported that AKAP7^{CD} can bind 5′AMP (Gold *et al.*, 2008). Ns2 and AKAP7 present similar

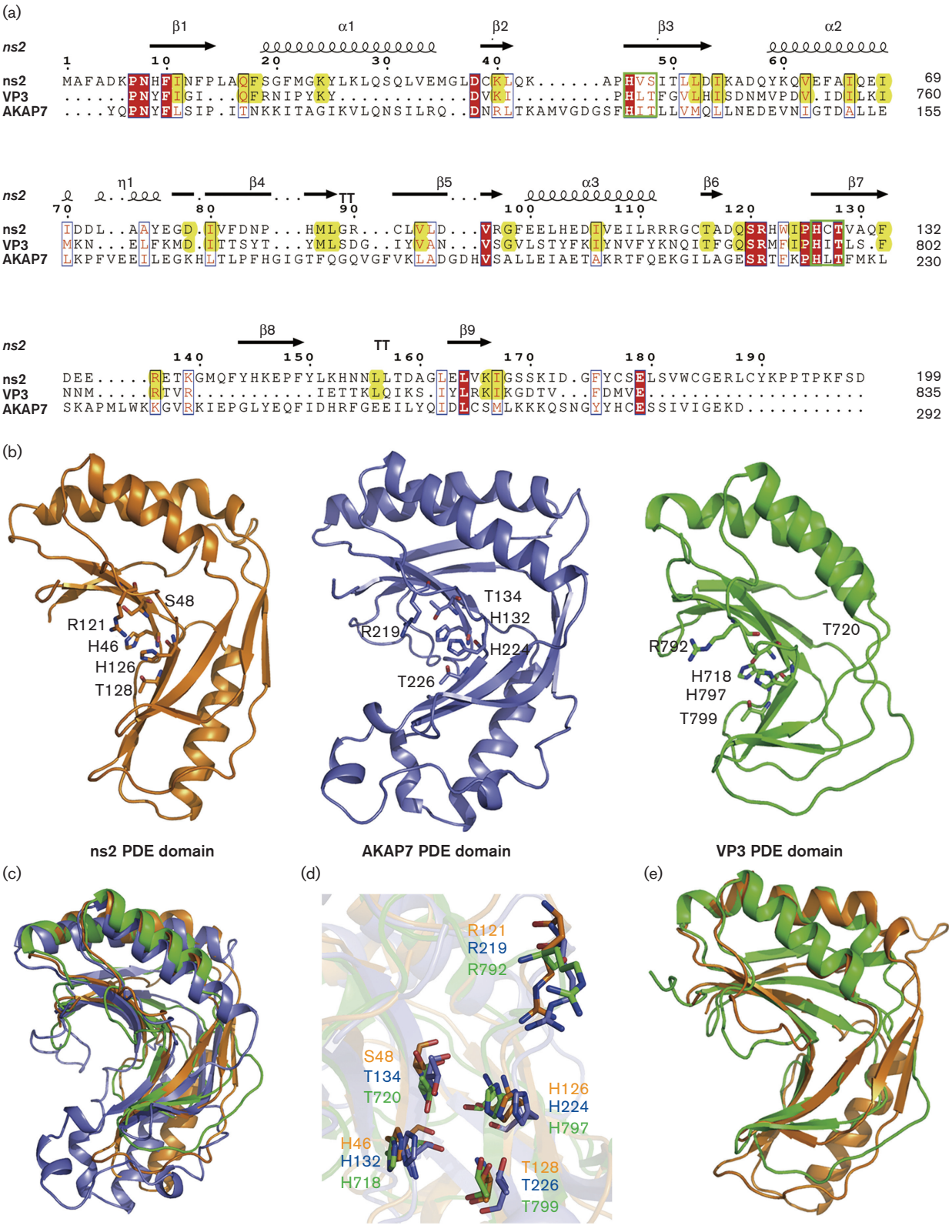

Fig. 2. Sequence and structural comparisons of ns2$^{7-167}$, AKAP7^{CD} and VP3-CTD. (a) Structure-based sequence alignment of the PDE domains of ns2$^{1-199}$, AKAP7^{CD} and VP3-CTD. Sequence comparison of rat AKAP7 (residues 76–292), MHV-A59 ns2 (residues 1–199) and rotavirus A VP3 (residues 697–835). The sequence homology of ns2$^{1-199}$ compared with AKAP7^{CD} and VP3-CTD was 13 % and 22 %, respectively (calculated by PDBeFold). Two conserved HxT/Sx motifs

(green box) and certain other conserved residues are labelled (red and yellow). The diagram was generated using ESPript 3.0. (b) Overview of the structures of $ns2^{7-167}$ (orange), $AKAP7^{CD}$ (slate) and VP3-CTD (green). Some conserved residues are shown using stick representation. (c) Structural alignment of $ns2^{7-167}$, $AKAP7^{CD}$ and VP3-CTD. The PDE domain structures of $ns2^{7-167}$, $AKAP7^{CD}$ and VP3-CTD were generally similar. (d) The two conserved HxT/Sx motifs at the H46/S48/H126/T128 residues of ns2 were located in coordinates similar to those of the H132/T134/H224/T226 residues of AKAP7 and the H718/T720/H797/T799 residues of VP3. The arginines in the R-loop were also conserved and display similar coordinates. (e) Structural alignment of $ns2^{7-167}$ and VP3-CTD showing high structural homology in the catalytic domain.

PDE domains and conserved key residues based on sequence or structural alignment. The structure of $AKAP7^{CD}$ binding to 5′AMP (PDB ID 2VFK) indicates that H224 from the second HxT/Sx motif forms a hydrogen bond with the bridging ester oxygen, and two threonines (T134/T226) from the two HxT/Sx motifs form hydrogen bonds with the phosphate oxygen atoms (Fig. 3a). The R219 in the R-loop region forms a cation–π interaction with the adenine moiety of 5′AMP of AKAP7 (Gold *et al.*, 2008). $Ns2^{7-167}$ showed similar residues, H46/R121/T128, in similar coordinates, with the only difference being the presence of a serine (S48) in ns2 (Fig. 3b). Both threonine and serine can present a hydroxyl group, which could potentially donate hydrogen bonds to the phosphate oxygen atoms of 5′AMP. From the published structure of VP3-CTD in complex with 2-5A (PDB ID 4YE2), it can be observed that the residues T720, H797 and T799 of the HxT/Sx motifs interact with 5′ monophosphate of the 5′ adenosine in 2-5A via hydrogen bonds (Fig. 3c, d) (Ogden *et al.*, 2015). H718 donates hydrogen bonds to the phosphate oxygen atom and further stabilizes 2-5A. R792 in the R-loop forms a cation-interaction with the adenine base of the substrate. These residues stabilize 2-5A. ns2 displays similar HxT/Sx motifs and residues at similar coordinates, which provide the structural basis for binding 2-5A (Fig. 3d). These structural features demonstrate a similar mechanism in degrading 2-5A.

Prior studies have reported that MHV ns2 and the cellular protein AKAP7 exhibit similar 2′,5′-PDE enzymic activity in degrading 2-5A (Gusho *et al.*, 2014). To compare the activities of these proteins and to verify the activity of the truncated ns2 used for crystallization, mammalian expression vectors pCAGGS and pCAGGS encoding $ns2^{1-199}$, $ns2^{1-199\ H126R}$, $AKAP7^{CD}$ and $AKAP7^{CD\ H224R}$ proteins with a C-terminal FLAG tag were individually transfected into 293T cells. At 48 h post-transfection, cells were collected and analysed by Western blotting. All of the proteins tested were expressed at high levels in human 293T cells (Fig. 3e). To compare the 2′,5′-PDE activity of truncated $ns2^{1-199}$ protein with that of the other proteins in intact cells, pCAGGS and pCAGGS plasmids encoding WT ns2, $ns2^{1-199}$, $ns2^{1-199\ H126R}$, $AKAP7^{CD}$ and $AKAP7^{CD\ H224R}$ were transfected into 293T cells. At 18 h after transfection, cells were treated with poly(rI) : poly(rC) to activate OAS. The cells were incubated for an additional 6 h before being harvested. Subsequently, 2-5A was isolated and then quantified using a fluorescence resonance energy transfer (FRET) assay as previously reported (Thakur *et al.*, 2005). We clearly demonstrated that $ns2^{1-199}$ cleaved 2-5A and that the mutant $ns2^{1-199\ H126R}$ protein lacked 2′,5′-PDE activity. Levels of 2′,5′-PDE activity were compared among $ns2^{1-199}$, full-length ns2, and $AKAP7^{CD}$ (Fig. 3f). The results demonstrated that full-length ns2 and the $AKAP7^{CD}$ displayed similar 2′,5′-PDE activity, whereas they lost catalytic activity after the key histidine was mutated. Truncated ns2 (residues 1–199) retained 2′,5′-PDE activity, although reduced compared with full-length WT ns2. It is possible that some residues in the carboxy-terminal domain of ns2 may enhance 2′,5′-PDE activity.

The structural analysis showed that the key residues in HxT/Sx motifs of ns2 protein were strictly conserved and located at similar coordinates compared with those of $AKAP7^{CD}$ and VP3-CTD. This structure also revealed that the conserved arginine in the R-loop region might play a key role in stabilizing the adenine moiety. These structural features suggest that these proteins bind and degrade 2-5A in a similar way. Based on the structural alignment of $ns2^{7-167}$, $AKAP7^{CD}$ and VP3-CTD, we demonstrate that $ns2^{7-167}$ exhibits features of both $AKAP7^{CD}$ and VP3-CTD, whereas $ns2^{7-167}$ and VP3-CTD show greater sequence and structural homology (Fig. 2a, e). Previously, it has been speculated that MHV and some other viruses acquired ancestral precursors of viral 2′,5′-PDE genes from their hosts. Homologous recombination might have occurred between the MHV genome and host RNA, thus endowing viruses with the ability to antagonize innate immunity by degrading 2-5A (Gusho *et al.*, 2014; Luytjes *et al.*, 1988). Here, we provide further evidence for this concept at the structural level.

The family *Coronaviridae*, a large family of viruses, have the largest genomes among RNA viruses. The precise mechanisms by which these viruses evade innate immunity are complicated and remain to be fully elucidated. Several emerging infectious disease outbreaks in recent years were caused by coronaviruses, including severe acute respiratory syndrome (SARS), porcine epidemic diarrhea virus and Middle East respiratory syndrome (MERS). MHV, MERS and SARS all belong to the betacoronavirus family. To our knowledge, the crystal structure of the truncated PDE domain of MHV ns2 is the first ns2 PDE domain structure of any coronavirus to be solved. By resolving and analysing the structure of $ns2^{7-167}$, we demonstrated the structural basis for binding with 2-5A and obtained insight into the mechanism by which MHV, and perhaps other coronaviruses, evades host innate immunity.

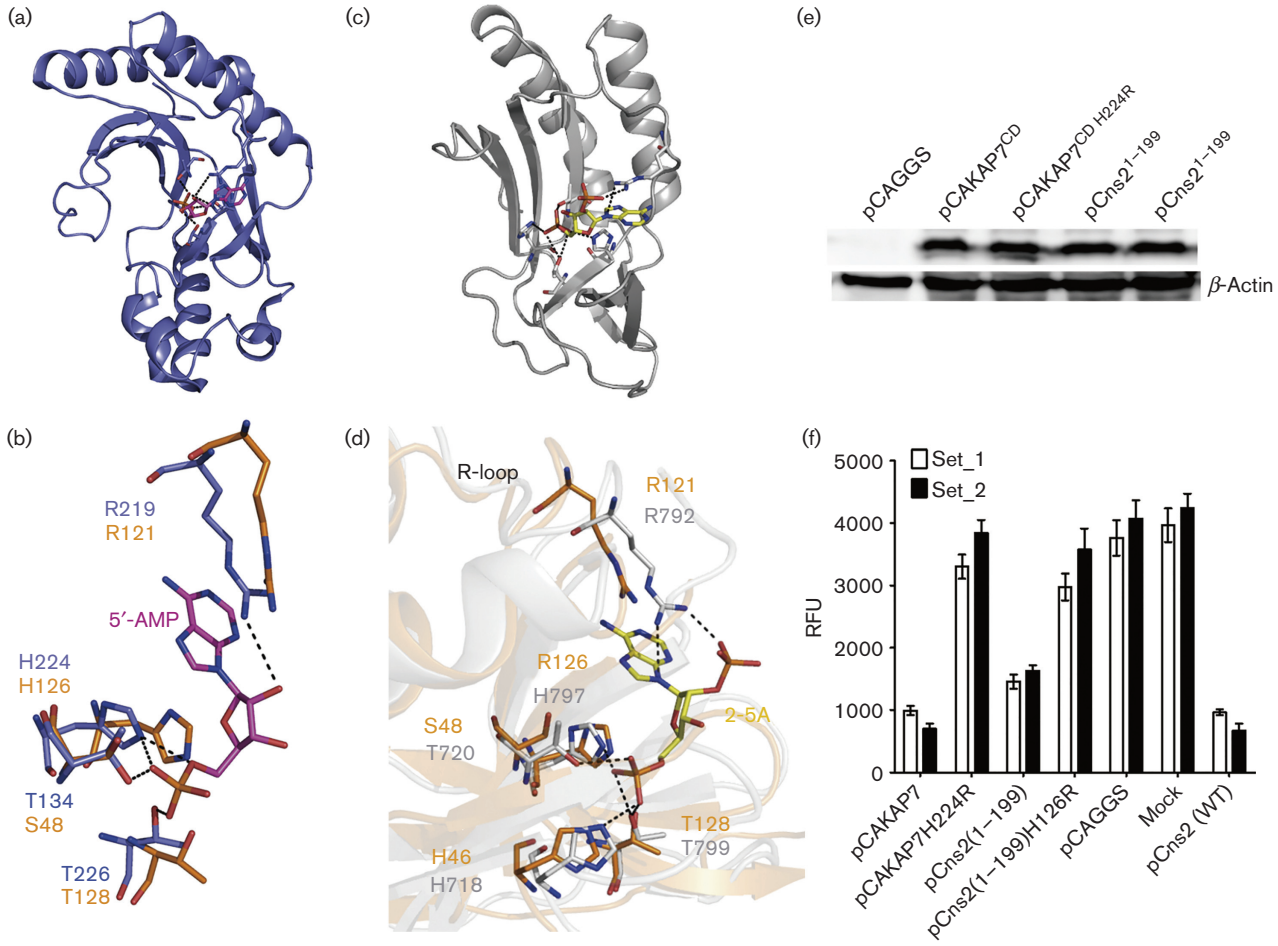

Fig. 3. Ns2$^{1-199}$ protein degrades 2-5A *in vivo* and has conserved residues compared with AKAP7^{CD} in complex with 5′AMP or VP3-CTD in complex with 2-5A. (a) Crystal structure of AKAP7^{CD} in a complex with 5′AMP (PDB ID 2VFK). AKAP7^{CD} structure-bound residues are shown as sticks, and 5′AMP is shown in magenta. (b) The conserved key residues used for binding 5′AMP in AKAP7^{CD} were compared with those of ns2$^{7-167}$. The residues of ns2$^{7-167}$ and AKAP7^{CD} are shown as sticks and labelled in orange or slate, respectively. (c) Crystal structure of VP3-CTD in complex with 2-5A (PDB ID 4YE2). 2-5A is shown in yellow. (d) The conserved key residues used for binding 2-5A in VP3-CTD were compared with those of ns2$^{7-167}$. The residues of ns2$^{7-167}$ and VP3-CTD are shown as sticks and labelled in orange and grey, respectively. (e) Western blot analysis of AKAP7^{CD}, AKAP7$^{CD\ H224R}$, ns2$^{1-199}$ and ns2$^{1-199\ H126R}$ proteins stably expressed in 293T cells. (f) Levels of 2-5A in 2 μg pIC ml^{-1} transfected into 293T cells expressing AKAP7^{CD}, AKAP7$^{CD\ H224R}$, ns2$^{1-199}$, ns2$^{1-199\ H126R}$, ns2 or empty vector in a 6 cm plate for 6 h. The results were determined using two biological samples (mean of three biological replicates and error bars represent standard deviation) labelled Set_1 and Set_2. RFU, Relative fluorescence units.

Acknowledgements

We thank the staff at the SSRF beam line BL17U1 for assistance with X-ray data collection. This work was partially supported by the National Natural Science Foundation of China (31372419) to L. Z. and NIH/NIAID grant AI104887 to S. R. W. and R. H. S.

References

Adams, P. D., Grosse-Kunstleve, R. W., Hung, L.-W., Ioerger, T. R., McCoy, A. J., Moriarty, N. W., Read, R. J., Sacchettini, J. C., Sauter, N. K. & Terwilliger, T. C. (2002). PHENIX: building new software for automated crystallographic structure determination. *Acta Crystallogr D Biol Crystallogr* **58**, 1948–1954.

Brandmann, T. & Jinek, M. (2015). Crystal structure of the C-terminal 2′,5′-phosphodiesterase domain of group A rotavirus protein VP3. *Proteins* **83**, 997–1002.

Cole, J. L., Carroll, S. S., Blue, E. S., Viscount, T. & Kuo, L. C. (1997). Activation of RNase L by 2′,5′-oligoadenylates. Biophysical characterization. *J Biol Chem* **272**, 19187–19192.

Der, S. D., Zhou, A., Williams, B. R. & Silverman, R. H. (1998). Identification of genes differentially regulated by interferon alpha, beta, or gamma using oligonucleotide arrays. *Proc Natl Acad Sci U S A* **95**, 15623–15628.

Desselberger, U. (2014). Rotaviruses. *Virus Res* **190**, 75–96.

Dong, B. & Silverman, R. H. (1995). 2-5A-dependent RNase molecules dimerize during activation by 2-5A. *J Biol Chem* **270**, 4133–4137.

Emsley, P. & Cowtan, K. (2004). Coot: model-building tools for molecular graphics. *Acta Crystallogr D Biol Crystallogr* **60**, 2126–2132.

Gold, M. G., Smith, F. D., Scott, J. D. & Barford, D. (2008). AKAP18 contains a phosphoesterase domain that binds AMP. *J Mol Biol* **375**, 1329–1343.

Gusho, E., Zhang, R., Jha, B. K., Thornbrough, J. M., Dong, B., Gaughan, C., Elliott, R., Weiss, S. R. & Silverman, R. H. (2014). Murine AKAP7 has a 2′,5′-phosphodiesterase domain that can complement an inactive murine coronavirus ns2 gene. *MBio* **5**, e01312–e01314.

Han, Y., Donovan, J., Rath, S., Whitney, G., Chitrakar, A. & Korennykh, A. (2014). Structure of human RNase L reveals the basis for regulated RNA decay in the IFN response. *Science* **343**, 1244–1248.

Heras, B. & Martin, J. L. (2005). Post-crystallization treatments for improving diffraction quality of protein crystals. *Acta Crystallogr D Biol Crystallogr* **61**, 1173–1180.

Hovanessian, A. G. & Justesen, J. (2007). The human 2′-5'oligoadenylate synthetase family: unique interferon-inducible enzymes catalyzing 2′-5′ instead of 3′-5′ phosphodiester bond formation. *Biochimie* **89**, 779–788.

Huang, H., Zeqiraj, E., Dong, B., Jha, B. K., Duffy, N. M., Orlicky, S., Thevakumaran, N., Talukdar, M., Pillon, M. C. & other authors (2014). Dimeric structure of pseudokinase RNase L bound to 2-5A reveals a basis for interferon-induced antiviral activity. *Mol Cell* **53**, 221–234.

Kerr, I. M. & Brown, R. E. (1978). pppA2'p5'A2'p5'A: an inhibitor of protein synthesis synthesized with an enzyme fraction from interferon-treated cells. *Proc Natl Acad Sci U S A* **75**, 256–260.

Kristiansen, H., Gad, H. H., Eskildsen-Larsen, S., Despres, P. & Hartmann, R. (2011). The oligoadenylate synthetase family: an ancient protein family with multiple antiviral activities. *J Interferon Cytokine Res* **31**, 41–47.

Luytjes, W., Bredenbeek, P. J., Noten, A. F., Horzinek, M. C. & Spaan, W. J. (1988). Sequence of mouse hepatitis virus A59 mRNA 2: indications for RNA recombination between coronaviruses and influenza C virus. *Virology* **166**, 415–422.

Ogden, K. M., Hu, L., Jha, B. K., Sankaran, B., Weiss, S. R., Silverman, R. H., Patton, J. T. & Prasad, B. V. (2015). Structural basis for 2′-5′-oligoadenylate binding and enzyme activity of a viral RNase L antagonist. *J Virol* **89**, 6633–6645.

Otwinowski, Z. & Minor, W. (1997). Processing of X-ray diffraction data collected in oscillation mode. *Methods Enzymol* **276**, 307–326.

Schindler, C. & Darnell, J. E., Jr. (1995). Transcriptional responses to polypeptide ligands: the JAK-STAT pathway. *Annu Rev Biochem* **64**, 621–652.

Silverman, R. H. (2007). Viral encounters with 2′,5′-oligoadenylate synthetase and RNase L during the interferon antiviral response. *J Virol* **81**, 12720–12729.

Silverman, R. H. & Weiss, S. R. (2014). Viral phosphodiesterases that antagonize double-stranded RNA signaling to RNase L by degrading 2-5A. *J Interferon Cytokine Res* **34**, 455–463.

Stark, G. R., Kerr, I. M., Williams, B. R., Silverman, R. H. & Schreiber, R. D. (1998). How cells respond to interferons. *Annu Rev Biochem* **67**, 227–264.

Thakur, C. S., Xu, Z., Wang, Z., Novince, Z. & Silverman, R. H. (2005). A convenient and sensitive fluorescence resonance energy transfer assay for RNase L and 2′,5′ oligoadenylates. *Methods Mol Med* **116**, 103–113.

Wang, Q. & Carmichael, G. G. (2004). Effects of length and location on the cellular response to double-stranded RNA. *Microbiol Mol Biol Rev* **68**, 432–452.

Zaki, A. M., van Boheemen, S., Bestebroer, T. M., Osterhaus, A. D. & Fouchier, R. A. (2012). Isolation of a novel coronavirus from a man with pneumonia in Saudi Arabia. *N Engl J Med* **367**, 1814–1820.

Zhang, R., Jha, B. K., Ogden, K. M., Dong, B., Zhao, L., Elliott, R., Patton, J. T., Silverman, R. H. & Weiss, S. R. (2013). Homologous 2′,5′-phosphodiesterases from disparate RNA viruses antagonize antiviral innate immunity. *Proc Natl Acad Sci U S A* **110**, 13114–13119.

Zhao, L., Rose, K. M., Elliott, R., Van Rooijen, N. & Weiss, S. R. (2011). Cell-type-specific type I interferon antagonism influences organ tropism of murine coronavirus. *J Virol* **85**, 10058–10068.

Zhao, L., Jha, B. K., Wu, A., Elliott, R., Ziebuhr, J., Gorbalenya, A. E., Silverman, R. H. & Weiss, S. R. (2012). Antagonism of the interferon-induced OAS-RNase L pathway by murine coronavirus ns2 protein is required for virus replication and liver pathology. *Cell Host Microbe* **11**, 607–616.